15TH IEA HEAT PUMP CONFERENCE
MAY 26–29, 2026 | HOFBURG
VIENNA 2026
DECARBONISATION THROUGH INNOVATION

Experimental study of latent heat storage integration in a heat pump refrigeration circuit

Brice Dubreil [a,*], Abdelouhab Labihi [b], José Lara Cruz [c], Jérôme Soto [d], Jean-Pierre Bedecarrats [c]

[a] Nobatek, 67 rue de Mirambeau, 64600 Anglet, France
[b] Pôle Cristal, 49 Av. René Cassin, 22100 Dinan, France
[c] Universite de Pau et des Pays de l'Adour, LaTEP, Bâtiment d'Alembert Rue Jules Ferry, 64075 Pau, France
[d] ICAM School of Engineering, Nantes Campus, 35 avenue du Champ de Manœuvres, 44470 Carquefou, France

Abstract

Heat pumps (HP) are an efficient way to reduce the carbon impact of the building sector, which represented about 34% of energy-related emissions in Europe in 2022. Air-source heat pumps (ASHP) represent the majority of HPs installed worldwide; however, their performance deteriorates significantly at low ambient temperatures. Raising the evaporation temperature should significantly improve the seasonal performance of an ASHP. In this study, an ASHP integrating a latent thermal storage that can replace the evaporator when outdoor conditions are unfavorable is studied. Energy is stored in the thermal storage by means of an additional heat exchanger that performs direct heat exchanges with the HP refrigerant. Warmest outdoor temperatures are used to charge the storage unit without impacting the system performance. A suitable Phase Change Material (PCM) has been selected based on its thermal features and its compatibility with the system and a prototype has been built to study the feasibility of such a system. The latent storage was able to efficiently store and release about $0.8\ kWh$ of thermal energy and raise the refrigerant evaporation temperature. An energy saving of 10% was observed when comparing the system in HP mode and in storage mode.

Selection and/or peer-review under the responsibility of the organizers of the 15th IEA Heat Pump Conference 2026.

Keywords: Heat pump; Latent thermal storage; Phase Change Material

1. Introduction

In Europe in 2022, the building sector was responsible for 34% of energy-related greenhouse gas emissions [1]. Reducing these emissions is essential to satisfy the requirements of the Paris Agreement [2] and more generally, to achieve a lower-carbon society. Among these 34% of emissions, part of it comes from the use of fossils fuels for heating, for example in gas boilers. Electrically driven Heat Pumps (HPs) are a suitable replacement for these heating systems. Thanks to low-carbon electricity, replacing a gas boiler with an HP can reduce emissions by a factor of ten in France, according to ADEME (French Environment and Energy Management Agency) [3].

HPs operate with a heat source, and the temperature of this source affects their performance, especially the Coefficient of Performance (COP). In particular, Air Source Heat Pumps (ASHPs) are very sensitive to the outdoor temperature, and they generally have the lowest average source temperature among the different types of heat pump [4]. Having a storage system capable of temporarily raising the evaporation temperature could be a solution to improve the system performance and reduce the impact of low outdoor temperatures.

This kind of system would require a heat storage unit with a stable temperature, capable of replacing outdoor air as a heat source. Phase-Change Materials (PCMs) offer this specific feature, by storing heat at near-constant temperature around their phase change temperature and showing important storage density [5]. The association

* Corresponding author
E-mail address: bdubreil@nobatek.com

of a latent thermal storage with an HP has been studied in recent years. Reviews from Gu et al. [6] and Osterman and Stritih [7] presented many different applications, with various designs and uses. Qu et al. [8] studied the integration of a latent heat storage in a cascade HP for defrosting, and managed to reduce the defrosting duration by 64% and the energy consumption by 30% compared to a standard hot gas by-pass method, while continuing to partially satisfy the heating need. Jin et al. [9] studied different operating strategies of an HP coupled with a latent storage integrated on the water distribution circuit, in order to enable demand-side management. Results showed that adding a latent storage alongside a sensible water storage may reduce operating costs under specific strategies. Charging the storage while the outdoor temperature was high reduced the system energy consumption.

Operating such system is a major concern, as it can significantly affect overall performance. In particular, outdoor air temperature is a key variable in the development of operating strategies. Hirschey et al. [10] evaluated how integrating thermal energy storage with heat pumps can reduce energy consumption and peak electricity demand by comparing hybrid systems with conventional ones across all temperature configurations. The maximum energy savings occur when storage and application temperatures are similar, while larger temperature differences enhance peak load reduction, especially under significant ambient temperature fluctuations. Using modeling and simulation, Othman et al. [11] demonstrated that properly designed storage strategies significantly reduce peak loads while maintaining system performance, highlighting the importance of charging timing and thermal management. Considering several US climate zones, they showed that better gains were achieved by charging the storage when the outdoor temperature exceeded $10°C$ and discharging it when it fell below $-5°C$.

To achieve more effective heat transfer with the PCM, several studies examined the possibility to directly integrate the storage module into the refrigeration circuit. The storage position then becomes a key aspect of the study. A storage placed on the demand side (condenser side for heating application and evaporator side for cooling application) allows to directly meet the demand for a short period of time, giving peak shaving capacity to the system. Yu [12] studied a floor heating numerical model where heat is stored during the day and used during the night to completely shut down the heat pump, thanks to direct discharge into the water distribution circuit. A similar experimental concept was made by Maaraoui [13] where the heat is discharged by circulating air through a three media condenser. The low conductivity of the PCM was compensated by the addition of a metal foam. This low conductivity issue is systematic and requires the use of heat transfer intensification techniques [14]. An experimental concept made by Palomba [15] considered a cold storage charged by the HP refrigerant evaporation and discharged using a water flow, offering the perspective of providing cooling while improving flexibility.

Conversely, placing the storage on the source side makes it possible to improve the source temperature and benefit from a better COP, especially when the outdoor conditions are extreme. Li [16] presented a numerical study where the heat from a sub-cooler is used to melt the PCM. The storage is later discharged by bypassing the outdoor evaporator during peak hours. This reduced by 25% the monthly cost of the system compared to a standard HP during December. Bastani [17] modeled a pipe-in-pipe heat exchanger with PCM, with two different refrigeration circuit architectures for heating: one with the storage associated series with the condenser and one in parallel. Charging time was shorter with the parallel configuration but resulted in a temperature stratification, while the phase-change was uniform in the series configuration.

This work presents an original experimental investigation of an air-source heat pump (ASHP) directly coupled with a latent heat thermal energy storage integrated into the refrigeration circuit. The latent storage operates as an active evaporator-side component, increasing the refrigerant evaporation temperature. Unlike most configurations, the experimental setup is able to perform in standard HP mode as well as in storage (charging/discharging) mode, thanks to several valves. Several experimental protocols were conducted to characterize the latent heat storage and to measure the system performance under various operating conditions, with particular emphasis on comparing the overall efficiency of the system with and without latent heat storage. Careful consideration is given to the heat transfer between the PCM and the refrigerant undergoing phase change within the latent heat exchanger, as well as to the effects of changing the HP heat source.

2. Experimental setup

2.1. General description

The experimental prototype consists of six main components : a reciprocating compressor operating with R134a (Embraco VNEK610Z, $0.95\ kW$ of cooling capacity at $10°C/35°C$, $2000\ RPM$), a water-refrigerant plate condenser, an air-refrigerant finned tube evaporator, a PCM-refrigerant heat exchanger, an expansion valve and a four-way valve.

The prototype is located in a climate-controlled environment, with the air-refrigerant evaporator exchanging heat with another climate-controlled chamber. The compressor is frequency-controlled, with a rotational speed varying between 2000 and 4500 rotations per minute. The plate condenser exchanges heat with a water loop in which both the flow rate and the inlet temperature are controlled.

Table 1. RT21HC thermo-physical properties [18]

Characteristic	Value	Unit
Melting temperature	20-23	$°C$
Congealing range	21-19	$°C$
Phase-change enthalpy	190 ± 7.5%	$kJ.kg^{-1}$
Density (solid/liquid)	0.88/0.77	$kg.L^{-1}$
Specific heat capacity	2	$kJ.(kg.K)^{-1}$
Thermal conductivity	0.2	$W.(m.K)^{-1}$
Volume expansion	14	%

The PCM-refrigerant heat exchanger consists of two finned tube heat exchangers with four 5 mm diameter tube rows connected in series and immersed in a tank containing $10\ kg$ of PCM. The tank is $550\ mm$ high, $350\ mm$ wide and $115\ mm$ deep. Tubes are in copper and fins in aluminum. The PCM is the RT21HC from Rubitherm, with a phase change temperature between 19 and $23°C$. Its properties are summarized in Table 1. The upper surface of the tank is left open to allow the PCM to expand during phase-change, and the side walls are reinforced to prevent bending during the volume expansion This exchanger is hereafter referred to as LHEX (latent heat exchanger, Figure 1.a).

The prototype is instrumented with multiple sensors. Two pressure sensors (Huba Control 520.933S03300N) measure the suction and discharge pressure of the compressor. Two PT-100 probes and one electromagnetic flow meter (Yokogama AXG015) respectively measure the water inlet and outlet temperature of the plate condenser and the volumetric flow rate in the water circuit. Eight T-type thermocouples placed on the tubes surface along the refrigeration circuit measure the inlet and outlet temperatures of the various components: plate condenser, finned tube evaporator, compressor, and LHEX. Thirteen T-type thermocouples are placed inside the LHEX along the refrigerant path. They are arranged in trios: one sensor is located on a tube bend, and the two others are in the nearby PCM region, outside the fins. An additional thermocouple is positioned between the two finned tube batteries. Figure 1.b describes the position of thermocouples inside the LHEX. Not all details are shown. The refrigerant does not circulate in the same direction whether the LHEX is being charged or discharged. Finally, one temperature sensor measures the ambient temperature of the chamber simulating the outdoor climate. The total electrical consumption (compressor and evaporator fan) is measured by an energy sensor. Refrigerant circuit sensors are visible on Figure 2.b. T-type thermocouples uncertainty is $\pm 0.5°C$, while PT-100 uncertainty is close to $\pm 0.1°C$. Electromagnetic flow meter accuracy is slightly below $\pm 0.4\%$.

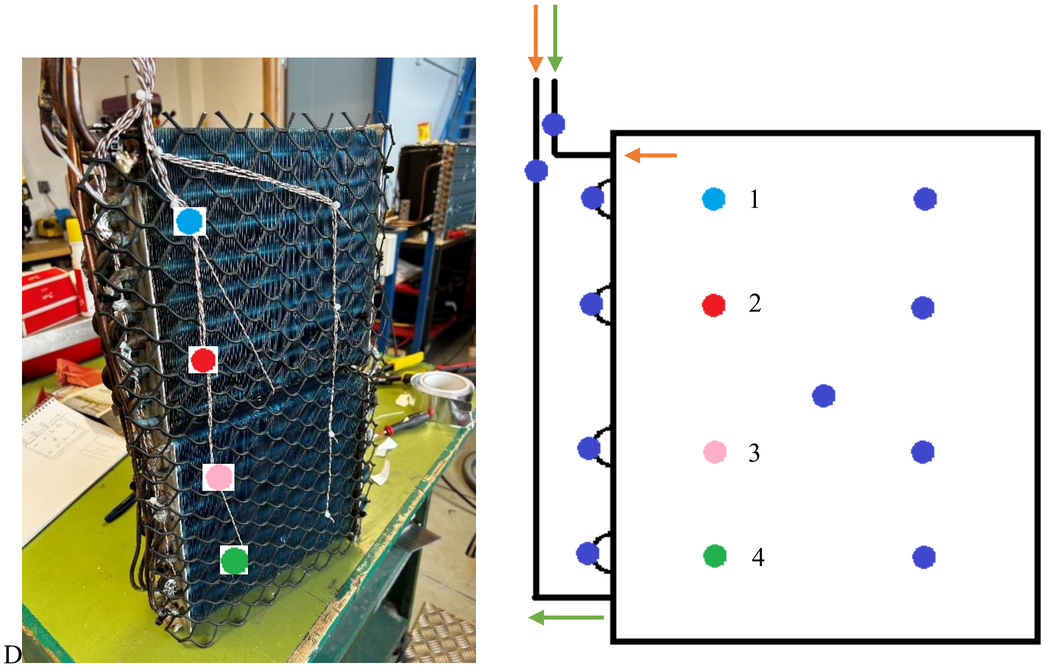

Fig. 1. Left (a): the instrumented latent heat exchanger. Right (b): the position of thermocouples. Green arrows: fluid direction in charging mode. Orange arrows: fluid direction in discharging mode.

2.2. Operating modes

The prototype operates in three modes, each one corresponding to a specific refrigerant circuit configuration. The first one corresponds to a standard HP cycle: outdoor air energy is absorbed by the refrigerant flowing through the evaporator and raised to a higher temperature by the compressor. It is then transferred to the water circuit through the condenser (Figure 2.a). This mode serves as a baseline for comparing system performance with and without latent storage. HP mode is operated with an outdoor temperature set to 5°C, simulating unfavorable outdoor conditions and highlighting the benefits of storage.

The second mode is the charging mode: it is similar to the first one, except that the heat produced is entirely transferred to the LHEX instead of the condenser. The PCM is thus heated above its melting temperature and melts. No heat is supplied to the water loop during this phase (Figure 2.b). Charging mode is operated with a favorable outdoor temperature (higher than 10°C), so as to avoid excessive performance degradation.

The third mode is the discharging mode: the air evaporator is bypassed, and the refrigerant evaporates inside the LHEX, resulting in a higher evaporation temperature compared to the HP mode when the outdoor temperature is low. Heat is then transferred to the water circuit through the condenser (Figure 2.c). The four-way valve and several manual valves (not shown on Figure 2) ensure the transition between the different operating modes. Mode transitions require approximately one minute to ensure proper distribution of the refrigerant charge throughout the circuit.

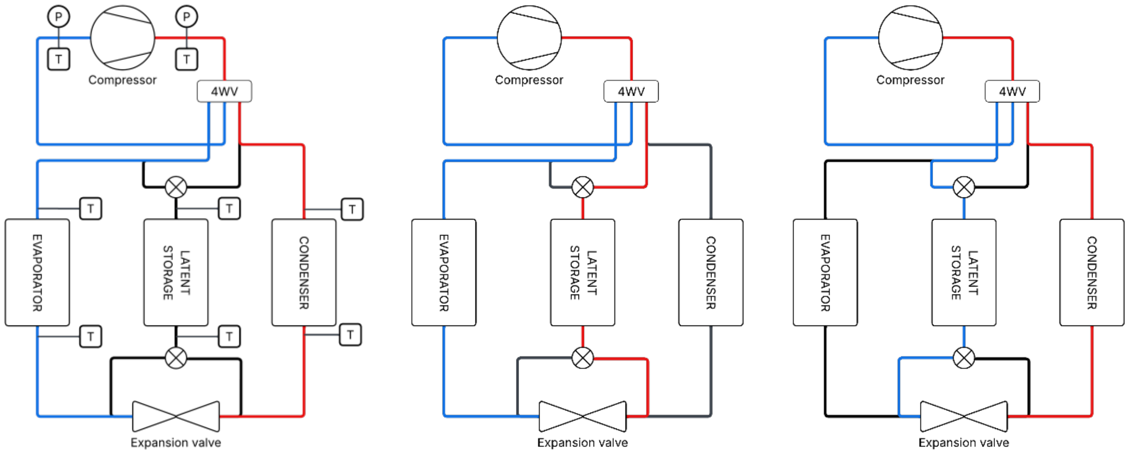

Fig. 2. Operating modes of the prototype. Left (a): standard HP mode; Middle (b): Charging mode; Right (c): Discharging mode. Black lines: no refrigerant circulation. Red lines: high pressure refrigerant. Blue lines: low pressure refrigerant.

For every mode, refrigerant enthalpies are calculated through the refrigerant circuit using *CoolProp* correlations [17] alongside pressure and temperature values. The compressor polynomials are known for this specific compressor model and make it possible to estimate the refrigerant flow rate as a function of the evaporation and the condensation temperatures, and the compressor speed. This allows us to calculate $\dot{Q}_{LHEX}$, the power charged or discharged from the LHEX with Eq. (1) and then the charged or discharged energy by integrating over time :

$$\dot{Q}_{LHEX} = \dot{m}_{ref}(t)|h_{out}(t) - h_{in}(t)| \tag{1}$$

$\dot{m}_{ref}$ is the refrigerant mass flow rate ($\mathrm{kg.s^{-1}}$), h_{in} and h_{out} respectively the inlet and outlet specific enthalpies of the LHEX ($J.kg^{-1}$).

For HP mode and discharging mode, the power $\dot{Q}_{supplied}$ (W) supplied on the water loop can also be calculated with Eq. (2):

$$\dot{Q}_{supplied} = \dot{m}c_{p_{water}}\Delta T_{water} \tag{2}$$

$\dot{m}$ is the water mass flow rate ($kg.s^{-1}$), $c_{p_{water}}$ the water specific heat capacity ($W.kg^{-1}K^{-1}$) and ΔT_{water} the water temperature gap between the outlet and the inlet (K).

Comparing the different modes is possible thanks to EEF in Eq. (3). This represents the amount of energy supplied by the system $E_{supplied}$ (J) to the water loop divided by the total energy consumed by the system E_{elec} (J), which includes compressor, water pump and evaporator fan electric consumption. The calculation method is similar to that used for the Seasonal Coefficient of Performance (SCOP):

$$EEF = \frac{E_{supplied}}{E_{elec}} = \frac{\int \dot{Q}_{supplied}(t)dt}{\int \dot{Q}_{elec}(t)dt} \tag{3}$$

$\dot{Q}_{elec}$ is the total consumed electrical power (W). It is also interesting to compare the instantaneous COP for the different modes with Eq. (4). $\dot{Q}_{heating}$ can be the charging power (charging mode) or the supplied power to the water loop (discharging and HP modes):

$$COP(t) = \frac{\dot{Q}_{heating}(t)}{\dot{Q}_{elec}(t)} \tag{4}$$

3. Results

3.1. Charging process

The melting process of the PCM is carried out in the charging mode. The compressor speed is set to $2000\ RPM$, which corresponds to its minimal speed. This prevents temperatures from rising too quickly near the refrigerant inlet of the LHEX, which could cause significant temperature stratification. The initial PCM temperature is adjusted to $10°C$ by means of the controlled climate in the chamber, ensuring a uniform initial temperature throughout the material. The outdoor air temperature is also set to $10°C$. The evolution of some temperatures within the storage unit is shown in Figure 3. Curve labelled “1” corresponds to a location near the refrigerant inlet, while “4” corresponds to the outlet region (Figure 1b). Colours correspond to Figure 1.b.

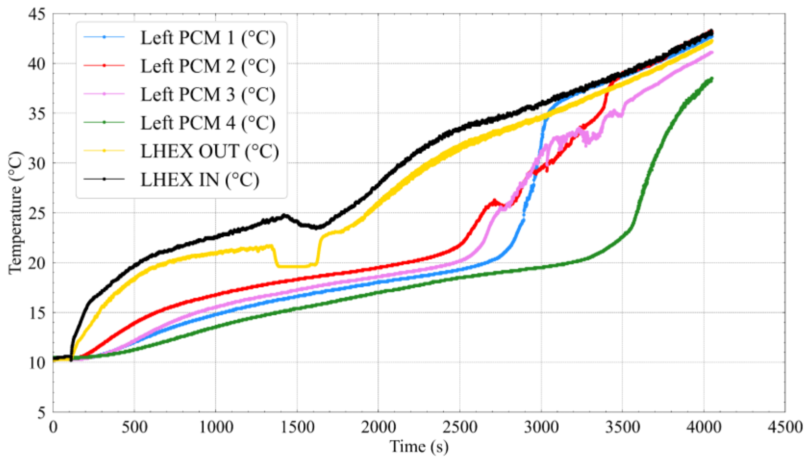

Fig. 3. PCM and LHEX inlet temperatures during the charging process.

During the initial seconds of the charging process, the temperatures rise rapidly as the PCM is still in a solid state solid and stores sensible heat. At $t = 1000\ s$, phase-change begins in the PCM, as shown by the occurrence of a temperature plateau in some curves. The material stores latent heat. The sequence of phase-change initiation does not perfectly follow the thermocouple numbering (“1” to “4”), since the sensors are located outside the fins and may have slightly shifted within the tank. At $t = 2500\ s$, some PCM regions are completely melted, and their temperature start to rise again, indicating sensible heat storage. The PCM can be considered fully melted at $t = 3300\ s$, meaning that for approximately 800 seconds, both liquid PCM and PCM undergoing phase change coexist inside the LHEX. At $t = 4000\ s$, a temperature stratification of about $5°C$ along the tank height is observed. The curves labelled “4” show a significant delay compared to the other six measurements, indicating that the PCM region farthest from the refrigerant inlet melts considerably later than the rest.

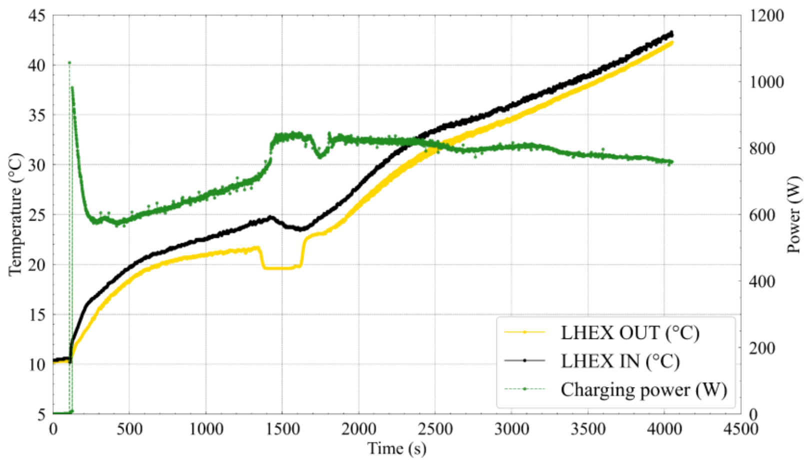

Fig. 4. LHEX charging power and inlet/outlet temperatures during charging process.

The charging power is shown in Figure 4. The refrigerant temperatures at the inlet (LHEX IN) and the outlet (LHEX OUT) of the LHEX are also shown. The sudden fall of the refrigerant outlet temperature at $t = 1350\ s$ indicates the occurrence of an important temporary subcooling. It means that the heat exchanged between the refrigerant and the PCM increases, as it is visible on the charging power curve. This increase in power may be attributed to the apparition of natural convection inside the PCM.

For the whole charging process, the stored energy value obtained by integrating Eq. (1) over time is $818\ Wh$. This energy is stored under two forms: sensible heat in the PCM, the fins and the tubes, and latent heat in the PCM. The theoretical value provided by Rubitherm for a $10\ kg$ PCM mass is $528 \pm 40\ Wh$. It corresponds to "a combination of latent and sensible heat in a temperature range of $13°C$ to $28°C$" [16]. The additional theorical sensible energy stored in the PCM over the ranges $10 - 13°C$ and $28 - 42°C$ is $94\ Wh$, bringing the total theorical energy stored in the PCM to $622\ \pm 40\ Wh$. Approximately $196\ Wh$ are therefore either stored in sensible energy in the LHEX metal parts or accounts for heat losses.

3.2. Discharging process

During the discharging mode, substituting the evaporator with the storage solidifies the PCM. The compressor speed is set at $2000\ RPM$, for the same reason as previously. In this case, the initial PCM temperature is set to 28°C, ensuring that the material is fully melted. The evolution of some temperatures inside the LHEX is shown in Figure 5. In this configuration, curve labelled "4" corresponds to a location near the refrigerant inlet, while "1" corresponds to the outlet.

Similarly to the charging process, the first few seconds are dedicated to sensible heat exchange. Phase-change begins at $t = 200\ s$ in the PCM regions closest to the refrigerant inlet. At $t = 500\ s$, the entire PCM is undergoing a phase-change. The process ends at $t = 1300\ s$ in the first affected regions and continues until $t = 2300\ s$, where all PCM regions are solidified. Unlike the melting process, the solidifying temperature range is extremely narrow, centered around $T = 22.5°C$.

At the end of the discharging process, the delay between the different phase-change fronts results in temperature stratification inside the LHEX. Applying the same method as for the charging process (time-integration of Eq. (1)), the experimentally measured released energy is estimated at $902\ Wh$ for the whole discharging period. The difference between the charging and the discharging energy can be explained by the measurement uncertainties and/or by the difference in the PCM temperature ranges, which implies that the stored sensible energy is not the same.

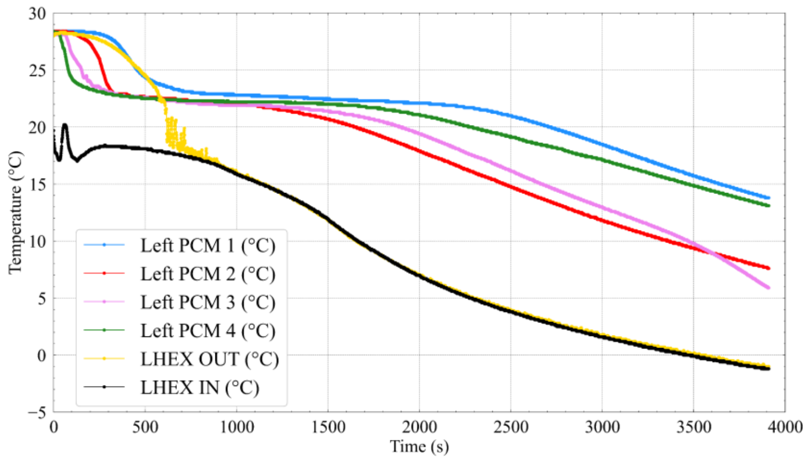

Fig. 5. PCM and LHEX inlet temperatures during the discharging process.

Figure 6 shows the discharging power, and the LHEX inlet and outlet refrigerant temperatures. Until $t = 600\ s$, the refrigerant fully evaporates in the LHEX, with a superheating reaching $10°C$. As the discharging power and the exchanged heat decreases, the refrigerant outlet temperature is the same as the inlet temperature, meaning that the evaporation is incomplete in the LHEX. The discharging power varies between $1200\ W$ and $500\ W$ at the end of the process.

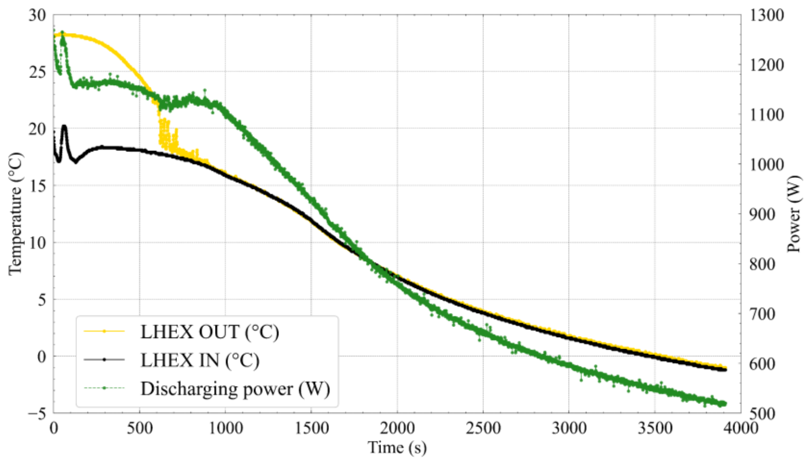

Fig. 6 . LHEX discharging power and inlet/outlet temperatures during discharging process.

3.3. Comparison between HP mode operation and storage mode operations

3.3.1. Complete storage cycle

In order to fully compare the storage architecture with a standard HP, a complete charge/discharge cycle must be performed. The outdoor air temperature is set at $15°C$ to simulate favorable outdoor conditions. At $t = 0\ s$, the LHEX temperatures are homogenised at $10°C$. The system is operated in charging mode until the minimum temperature within the LHEX exceeds $35°C$, at which point the storage can be considered fully charged. The system is then switched to discharging mode. The water volumetric flow rate is set to $1.5\ L/min$, and the LHEX is discharged until the maximum temperature drops below $15°C$. Throughout the entire process, the compressor speed remains constant at $2000\ RPM$, to avoid a significant temperature stratification inside the PCM. Some PCM temperatures are shown in Figure 7, along with the condensation and evaporation pressures.

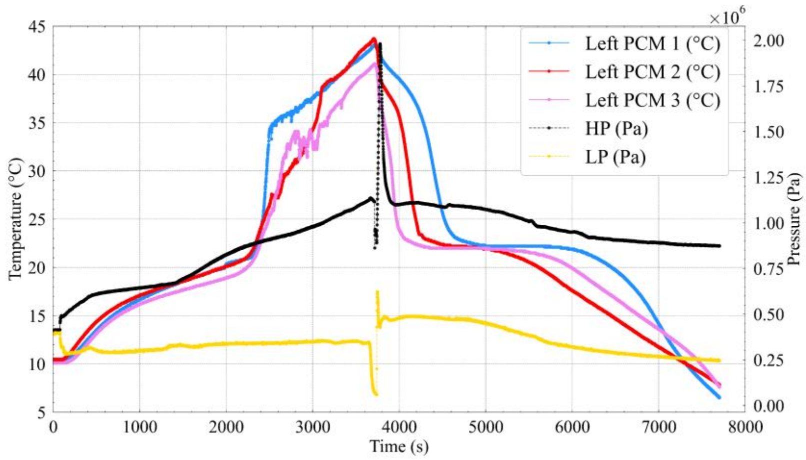

Fig. 7. Temperatures inside the LHEX and operating pressures during a complete charge/discharge cycle.

The charging period runs from $t = 0\ s$ to $t = 3660\ s$ and the discharging period from $t = 3780\ s$ to $t = 7700\ s$. These intervals are used to determine the consumed and supplied energy. The consumed energy is obtained by integrating over time the electrical power drawn by the compressor, the evaporator fan and the water pump. The supplied energy corresponds to the supplied power (Eq. (2)) integrated over time. The $120\ s$ period between the charging and discharging periods is not taken into account. During this two-minutes period, the system is manually operated to ensure proper refrigerant distribution in the circuit, causing brief pressure fluctuations.

Figure 8 illustrates the power variations within the system. The supplied power remains zero during the charging process. At $t = 3780\ s$, it rises to $1250\ W$ and then gradually decreases to $400\ W$. The total supplied energy is equal to $878\ Wh$.

The first portion of the storage power, determined with Eq. (1), corresponds to the LHEX charging power, which remains relatively stable at around $800\ W$. The second portion corresponds to the discharging power, i.e. the refrigerant evaporation power during discharge. Its profile follows that of the supplied power. During the whole process, the consumed power ranges between $200\ W$ and $400\ W$, resulting in a total consumed energy of $501\ Wh$. The EEF of the complete charge/discharge cycle is 1.75. Only the supplied energy is considered; the heat delivered to the LHEX during charging is not included.

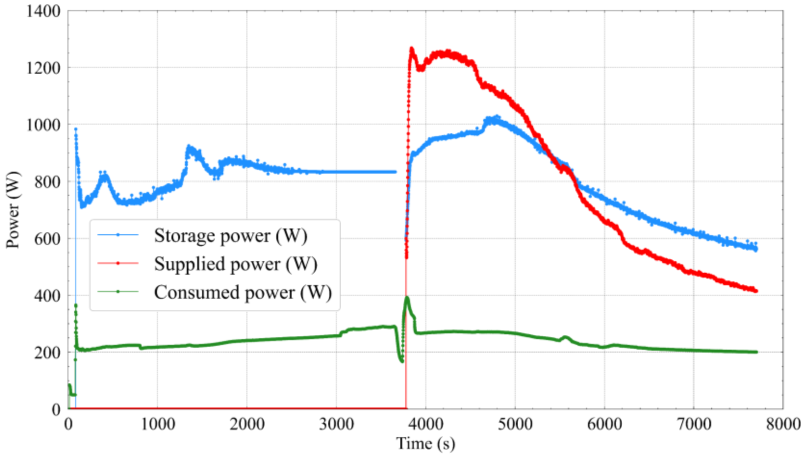

Fig. 8. Storage, supplied and consumed powers during the complete charge/discharge cycle.

3.3.2. HP mode performances

A test is carried out to evaluate the system's performance in HP mode. The system is operated in HP mode. The outdoor air temperature is set to $5°C$, to simulate unfavorable outdoor conditions, and the compressor speed is fixed at $4000\ RPM$ and the water volumetric flow rate is maintained at $1.5\ L/min$. The compressor speed is higher than in the charging and discharging modes. Since the LHEX is not used, there is no risk of excessive temperature stratification, and the compressor operates more efficiently at this speed. The results are shown in Figure 9. All the periodic fluctuations in the HP mode curves come from the setpoint temperature of the water temperature at the condenser inlet, which varies slightly around $28°C$. The supplied power, measured with Eq. (2), is slightly below $1\ kW$. The EEF is 1.57. For a meaningful comparison with the complete charge–discharge cycle, the supplied energy must be the same. To deliver $878\ Wh$, the system operating in HP mode will therefore consume $559\ Wh$.

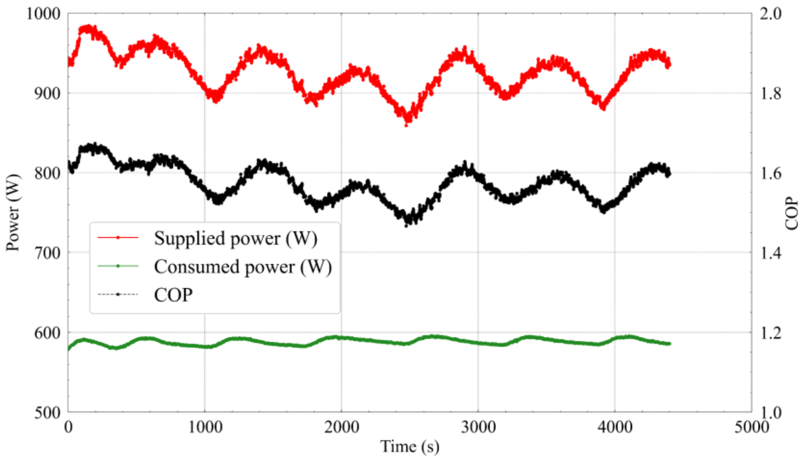

Fig. 9. Consumed and supplied powers for the standard HP mode, with system COP.

3.3.3. Comparison between HP mode and complete storage cycle

Figure 10 compares the evaporation pressure in discharging mode and in HP mode, along with their respective COP. In discharging mode, the refrigerant evaporates due to the heat transfer with the PCM, resulting in a higher evaporation temperature. During discharge, this temperature ranges from $15°C$ down to

$-5°C$, whereas in HP mode it remains relatively stable at $-2.5°C$. In discharging mode , the system achieves a higher COP than in HP mode for the whole discharge period.

The detailed values of supplied and consumed energies are presented in Table 2. For the same delivered energy, the energy consumption of the LHEX (complete charge/discharge cycle) configuration is 10.4% lower than that of the standard HP.

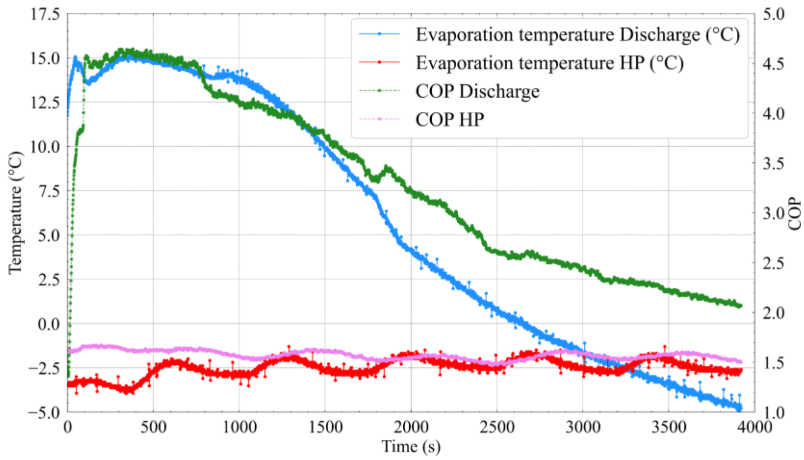

Fig. 10. Comparison of the evaporation temperature and the COP between the discharging and the HP mode.

Table 2. Comparison of *EEF,* supplied energy, and consumed energy between the LHEX and HP configurations.

		LHEX	HP
Supplied energy (Wh)		878	878
Consumed energy (Wh)	charge	241	559
	discharge	260	
	total	501	
EEF		1.75	1.57

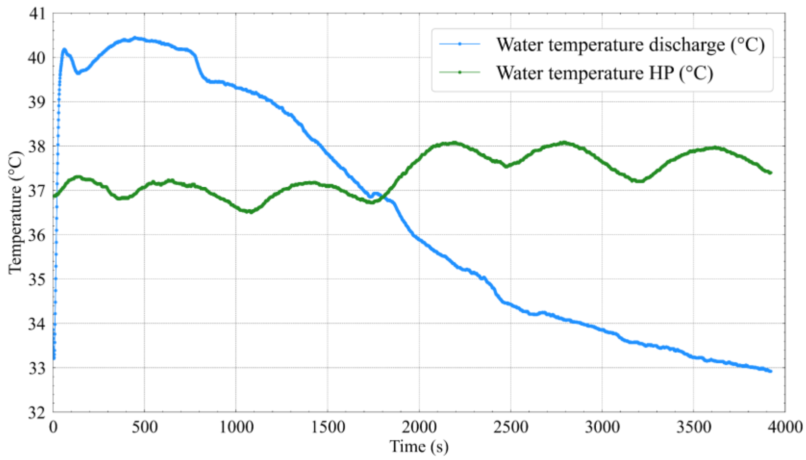

Fig. 11. Water temperature for both discharging and HP mode.

During discharge, the supplied power gradually decreases. Since the water flow rate is the same in both cases, the difference is due to the water temperature at the condenser outlet. Figure 11 shows this temperature for both discharging and HP modes. While the water temperature remains relatively constant at $37.5°C$ in HP mode, it decreases from $40.5°C$ to $33°C$ during discharging mode.

4. Conclusions, limits and perspectives

An original experimental setup of an ASHP integrating a latent heat storage on the refrigerant circuit was investigated in this study. The LHEX consisted of a finned tube heat exchanger immersed in a PCM, allowing direct heat exchange with the HP refrigerant. The system operates in three different modes. Charging and discharging modes were compared to standard HP mode. The LHEX was able to store between 0.8 and $0.9\ kWh$ of thermal energy and discharge the same amount over 1.1 hours.

Compared to a standard HP mode, the complete charge/discharge cycle demonstrated a 10.4% reduction in electrical energy consumption, while delivering the same amount of energy to the water loop. However, the water temperature was not stable during the discharge, highlighting the need for dynamic control, either for water flow or compressor speed. Moreover, this system contains significantly more refrigerant than a standard HP circuit, which can cause issues with refrigerant charge distribution between the different components. With regard to potential commercialization, refrigerant regulatory constraints could also restrict the range of feasible applications, by forcing the system to be located outdoors. Further experiments under dynamic outdoor temperatures will enable evaluation of the system under more realistic operating conditions. In particular, thermal losses of the LHEX were not investigated in this study and could become significant over longer storage periods.

5. Acknowledgements

This work was supported in the case of MCPAC project granted by the Nouvelle Aquitaine Region in the framework of the joint research team between the University de Pau et des Pays de l'Adour and Nobatek. This project is conducted in partnership with Pôle Cristal, ICAM Nantes and Danfoss, with the financial support of the Regional Council of Bretagne and the European Union (FEDER).

References

[1] IEA, 2022. The future of Heat Pumps. https://www.iea.org/reports/the-future-of-heat-pumps
[2] UN, The Paris Agreement, 2015. Paris Agreement to the UN Framework Convention on Climate Change.
[3] ADEME, 2023. Calculate the carbon impact of your heating, https://impactco2.fr/outils/chauffage
[4] Deng J., Wei Q., Liang M., He S., Zhang H., 2019. Does heat pumps perform energy efficiently as we expected: Field tests and evaluations on various kinds of heat pump systems for space heating. Energy and Buildings 182, p. 172-186.
[5] Jouhara H., Żabnieńska-Góra A., Khordehgah N., Ahmad D., Lipinski T., 2019. Latent thermal energy storage technologies and applications: A review. International Journal of Thermofluids 5-6, p. 100039.
[6] Gu H., Chen Y., Yao X., Huang L., Zou D., 2023. Review on heat pump (HP) coupled with phase change material (PCM) for thermal energy storage, Chemical Engineering Journal 455, p. 140701.
[7] Osterman E., Stritih E., 2021. Review on compression heat pump systems with thermal energy storage for heating and cooling of buildings, Journal of Energy Storage 39, p. 102569.
[8] Qu M., Qin R., Tang Y., Fan Y., Li T., 2017. An Experimental Study on the Improvement of Reverse Cycle Defrosting Performances for a Cascade Air Source Heat Pump using Thermal Energy Storage Based Defrosting Method, Procedia Engineering 205, p. 818-825.
[9] Jin X., Zheng S., Huang G., Ck Lai A., 2023. Energy and economic performance of the heat pump integrated with latent heat thermal energy storage for peak demand shifting, Applied Thermal Engineering 218, p. 119337.
[10] Hirschey J., Li Z., Gluesenkamp K. R., LaClair T., Graham S., 2023. Demand reduction and energy saving potential of thermal energy storage integrated heat pumps, International Journal of Refrigeration 148, p. 179-192.
[11] Othman A., Aute V., Tancabel J., 2024. Recharge Demand Mitigation for Latent Heat Thermal Energy Storage at Off-Peak Hours, International High Performance Buildings Conference. Paper 453.
[12] Yu M., Zhang C., Fan Y., Zhang X., Zhao Y., 2021. Performance study of phase change charging/discharging processes of condensing heat storage in cold regions based on a mathematical model, Applied Thermal Engineering 182, p. 115805.
[13] Maaraoui S., 2013. Étude et conception d'une pompe à chaleur résidentielle intégrant un stockage par chaleur latente, Thesis of Ecole Nationale Supérieure des Mines de Paris.
[14] Choure N., Alan T., Kumar R., 2023. A review on heat transfer enhancement techniques for PCM based thermal energy storage system, Journal of Energy Storage 72, p.108161.
[15] Palomba V., Varvagiannis S., Monokrousou E., Nitsch B., Barmparistas N., Bonanno A., Dino G. E., Leontaritis A., Strehlow A., Karellas S., Frazzica A., Cabeza L. F., 2021. Experimental evaluation of a heat pump-latent storage system for increasing renewable share of the residential stock, 13th IIR Conference on Phase-Change Materials and Slurries for Refrigeration and Air Conditionning, Italy.

[16] Li Z., Catano J., Gluesenkamp K., Shen B., LaClair T., Comparin R., Welch D., 2022. Simulation of a PCM Integrated Heat Pump Using Time-of-Use Utility Structure based Control Strategy for Demand Response, 19th International Refrigeration and Air Conditioning Conference, Italy.
[17] Bastani A., Tamasauskas J., 2023. Air-Source Heat Pump with Integrated Latent Heat Storage for Residential Buildings: Concept Development and Design Evaluation, Proceedings of the International Renewable Energy Storage Conference (IRES 2022), p. 29-46.
[18] Rubitherm, RT21HC Datasheet, https://www.rubitherm.eu/media/products/datasheets/Techdata_-RT21HC_EN_09102020.PDF
[19] Bell I., Wronski J., Quoilin S., Lemort V., 2014. Pure and Pseudo-pure Fluid Thermophysical Property Evaluation and the Open-Source Thermophysical Property Library CoolProp, Industrial and Engineering Chemistry Research 53, p 2498-2508.